Paper 3750-37, for presentation at SPIE Conference: **Earth Observing Systems IV,** July 1999, Denver, CO

Vacuum window optical power induced by temperature gradients

David R. Hearn[†]

MIT Lincoln Laboratory
244 Wood Street, Lexington, MA 02173

ABSTRACT

The Advanced Land Imager (ALI) of the EO-1 satellite has been calibrated under its normal operating conditions in a thermal vacuum chamber. The optical equipment for the calibrations had to be placed outside the chamber. The effects on the calibrating beam of the vacuum chamber window are described here. Since the instrument senses the reflected solar spectrum, the existing fused-silica window was found to have adequate spectral transmission properties. It also was measured to cause little wavefront error by itself (0.012 waves rms at 633 nm). When the chamber is under vacuum, and the interior cold shroud is cooled to ~ 100 K, the window develops significant optical power. This is a result of radiational cooling of the window, coupled with change of its index of refraction with temperature. Such an effect seriously compromises the spatial calibrations of the instrument, particularly MTF measurements. This effect was overcome in two ways: A heating plate placed outside the window was used to alter the temperature distribution until its effect on the wavefront was negligible. The more practical solution was to measure the window power with an interferometer, and compensate for it by shifting the target reticle of the collimator.

Keywords: opto-thermal effects, calibration, imaging, MTF, thermal/vacuum testing

1. INTRODUCTION

The need to calibrate the Advanced Land Imager (ALI) instrument of the EO-1 satellite under the correct operating conditions required that the instrument be placed in a thermal vacuum chamber. Spectral, radiometric, and spatial calibrations were performed there. All of the optical equipment for the calibrations was situated outside of the chamber, for several reasons. Even if the chamber were large enough to fit the required components, calibration equipment inside the chamber would have to operate under the same thermal/vacuum conditions as the instrument. Furthermore, it would be required to have minimal out-gassing properties so as not to contaminate the instrument or degrade the vacuum. Outside the chamber, in a normal clean-room environment, standard laboratory components could be used.

With the calibrating equipment outside the chamber, a window had to be interposed between that equipment and the instrument. An essential part of the calibration process is thus the characterization of the optical properties of this window. The window should have a high transmission throughout the spectral range of the instrument under test. If the instrument is to be used for imaging, it should have a high-quality optical figure, to minimize transmitted wavefront error (WFE). In particular, it should have little or no optical power.

The thermal vacuum chamber that was used to calibrate the ALI already had a window of fused silica, with a clear aperture of 30.48 cm (12 inches). Since the ALI operates in the reflected-solar spectral range (0.4 – 2.5 μm), this window was expected to have adequate spectral transmission. The following two sections describe the results of spectral transmission and optical figure measurements performed on the window. However, this paper is principally concerned with the optical power of the

---

This work was sponsored by NASA/Goddard Space Flight Center under U. S. Air Force Contract F19628-95-C-0002.

Opinions, interpretations, conclusions, and recommendations are those of the author and are not necessarily endorsed by the United States Air Force.

[†] Correspondence: Email: drhearn@ll.mit.edu; Telephone: 781-981-0918; Fax: 781-981-0969

window. When the thermal shroud (or cold wall) of the chamber is cooled, the window is also radiatively cooled. Since the perimeter of the window is firmly held by the warm tank wall, thermal gradients develop in the window material. This material changes its index of refraction with changing temperatures. As a result, the window develops optical power, depending on the exact configuration and thermal settings within the chamber. We have developed techniques to measure this power, and to overcome its effects. They are the topic of Section 4.

2. SPECTRAL TRANSMISSION

Although the window had originally been specified as fused silica, it was no longer known what grade of the material had been employed. Accordingly, transmission measurements were carried out, with an Oriel model MS257 double monochrometer operated in subtractive configuration. The light source was a 250 W quartz tungsten halogen lamp. The measured spectral transmission of the window is plotted in Figure 1.

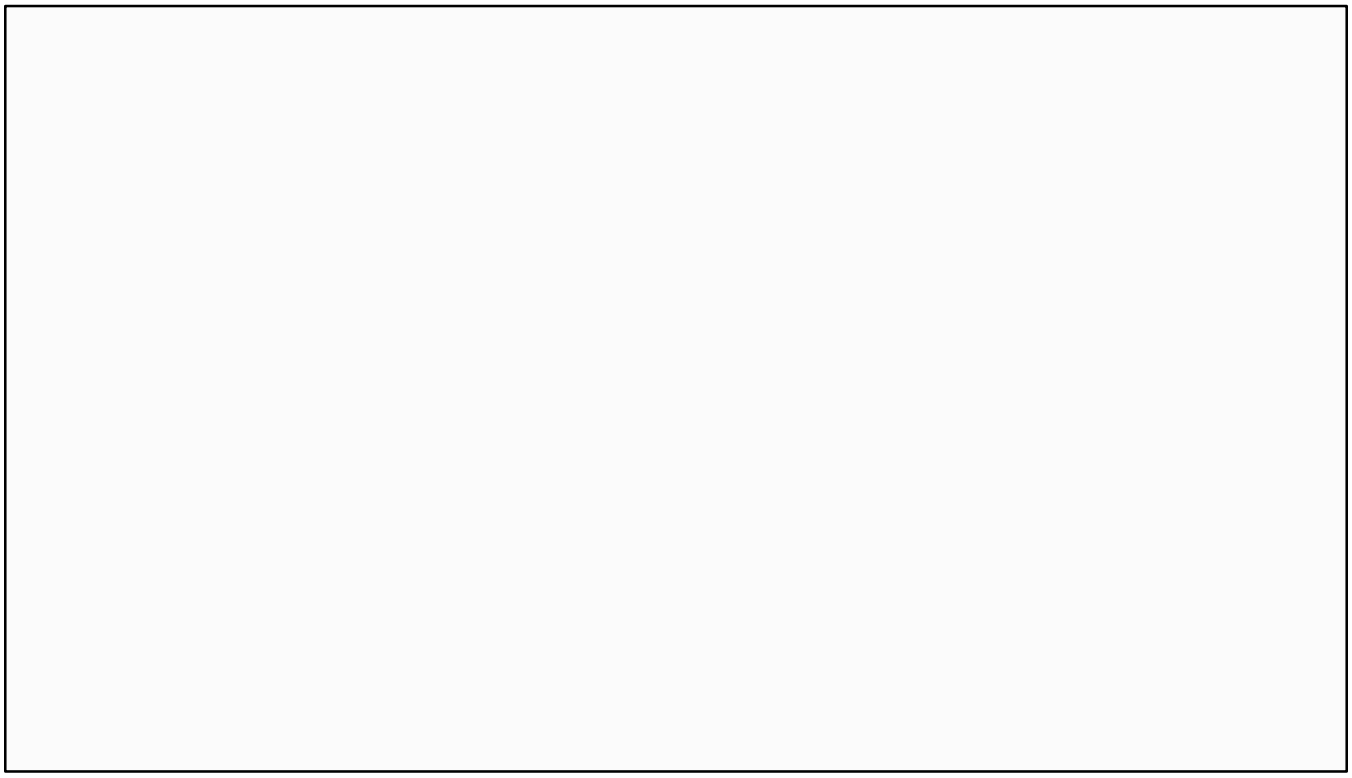

Figure 1. Spectral transmission of the vacuum window used during the calibrations of the EO-1 Advanced Land Imager.

3. OPTICAL FIGURE

The transmitted wavefront error (WFE) of the window was characterized with a Zygo Mark IV Fizeau interferometer, equipped with a 6-inch beam expander, and a 12-inch reference flat mirror behind the window. The reference flat mirror alone showed a WFE of 0.37 waves peak-to-valley (p-v), and 0.03 waves rms at 0.633 nm. For the transmitted WFE measurements, the WFE of the reference mirror was stored and subtracted from the window wavefront. The window was found to have a wedge of 7.2 arc seconds between the front and back faces. Since the Zygo beam could not span the entire aperture to be used, several overlapping interferograms were made. The computed wavefront errors in transmission (single pass) ranged from 0.053 waves p-v (0.005 waves rms) to 0.083 waves p-v (0.012 waves rms) at 0.633 nm, over the 6-inch apertures. Typical interferograms taken during these tests are shown in Figure 2.

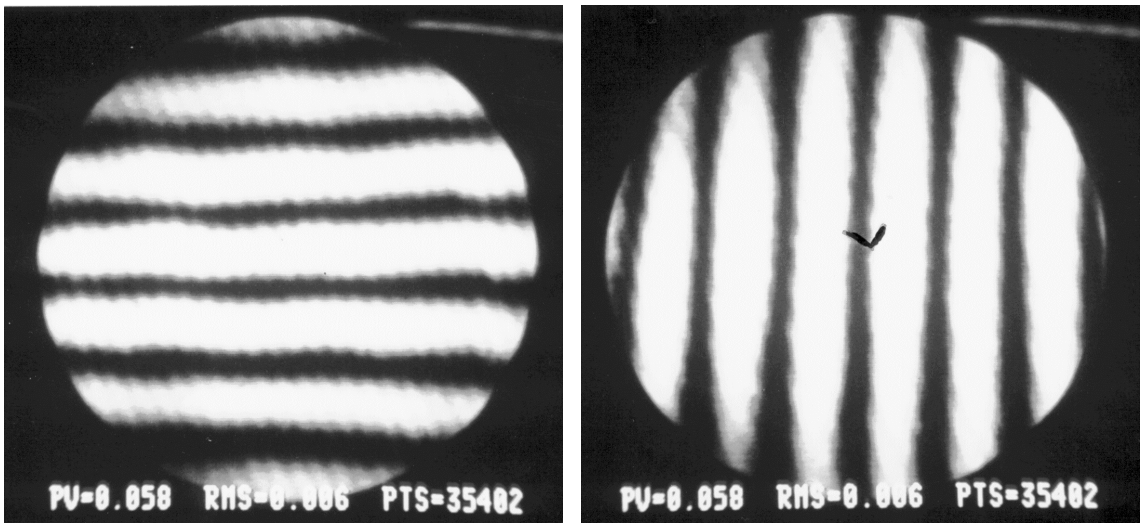

Figure 2. Interferograms of the vacuum window. The central six inches of the window are shown here. The dark "V" seen among the vertical fringes marks the center of the window.

4. OPTICAL POWER

While the window displayed little or no optical power when measured in isolation, several effects could alter its power when it is used on the vacuum system. When the system is evacuated, the window deflects into a meniscus shape under atmospheric pressure. When the cold shroud of the chamber interior is cooled, the window is cooled by radiation into the shroud. Both axial and radial temperature gradients develop within the window. Vukobratovich[1,2] has described the optical effects of these gradients. The following subsections show the magnitude of the effects in this case. Then we present the means by which the optical power developed in the window was measured and compensated.

4.0. Deflection of the window under atmospheric pressure

The axial deflection of the window surface at radius r caused by a pressure differential Dp may be expressed as[3]:

$$w(r) = \frac{3Dp(1-n^2)}{16EL^3}\left[\frac{5+n}{1+n}a^2 - r^2\right]\left[a^2 - r^2\right] \quad , \tag{1}$$

where

L = the thickness of the window = 0.0508 m,
a = the radius at which the window is simply supported = 0.16 m,
n = Poisson's ratio = 0.164, and
E = the elastic modulus of the window = 72.60 GPa.

Inserting the numerical constants, we have in units of meters,

$$w(r) = 1.94 \times 10^{-3}\left[4.44a^2 - r^2\right]\left[a^2 - r^2\right] \quad . \tag{2}$$

The deflection of the center of the window under vacuum is just 5.7 μm. The curvature of either side of the window near the axis is approximately

$$\frac{1}{R} \approx \frac{3(1-n)(3+n)a^2}{4EL^3}Dp \quad . \tag{3}$$

The lens constant of the system of air, window, and vacuum, with indices n_{air}, n_w, and 1, respectively, is given by

$$k = \frac{n_{air} - 1}{R} + \frac{L}{R^2} \cdot \frac{(n_w - 1)^2}{n_w} = \frac{n_{air}}{f_{air}} = \frac{1}{f_{vacuum}} \quad , \tag{4}$$

where for air in the laboratory at 1 atm, 21° C, 580 nm wavelength,

$$n_{air} - 1 \approx 2.73 \times 10^{-4} \quad .$$

Inserting this value, and the window index (1.4588 at 580 nm), we find that the lens constant is dominated by the first term, and has a value of 1.5×10^{-7} diopters. This is negligible in comparison with the uncertainty in the focus adjustment of a collimator.

4.1. Temperature distribution and optical power

A non-uniform temperature distribution in the window affects its optical properties in several ways. First, an axial gradient causes the window to assume a meniscus shape, as the colder side contracts relative to the warm side. Second, a radial gradient causes the cooler central portion to became thinner, forming a negative lens. Third, the index of refraction varies with temperature, forming a gradient-index lens. For fused silica near room temperature, the thermo-optic coefficient *dn/dT* is 9.90×10^{-6} K^{-1}.

For a purely axial temperature gradient, we find the lens constant to be

$$k = -\frac{(a_{TE} DT)^2}{L} \left[\frac{n_w - 1}{n_w} + \frac{n_{air} - 1}{a_{TE} DT} \right] \tag{5}$$

where

a_{TE} = the coefficient of thermal expansion = 5.10×10^{-7} K^{-1}, and
DT = the temperature difference from the front to the back faces of the window.

For a temperature difference of 3.5 °C in this instance, the values of the two terms in equation (5) are approximately -2×10^{-11} and -10^{-8}, respectively. The axial temperature gradient thus also has a completely negligible effect on the transmitted wavefronts.

The optical power resulting from a parabolic radial temperature gradient is given in reference 1 as

$$\frac{1}{f} = 8 \frac{L}{D^2} DT \left[(n-1)(1+n) a_{TE} + \frac{dn}{dT} \right] \quad . \tag{6}$$

More generally, the optical path difference as a function of radius across the window can be found as

$$OPD = \left[(n-1)(1+n) a_{TE} + \frac{dn}{dT} \right] \int_0^L [T(z) - T_A] dz \quad , \tag{7}$$

where the integration is along a path parallel to the optical axis.

4.2. Temperature distribution within the window

In order to understand fully the optical effects of the non-uniform window temperature, we have solved the diffusion equation:

$$\nabla^2 T = \frac{1}{a^2} \frac{\partial T}{\partial t} \quad , \tag{8}$$

where T is the temperature within the window, and a^2 is the thermal diffusivity of the material. We solved this partial differential equation in cylindrical coordinates, subject to the following definitions and simplified boundary conditions:

$$T = T_A + D \tag{9}$$

$$D = 0 \quad , \qquad for \;\; r = D/2 \, , \tag{10a}$$

$$k\frac{\partial D}{\partial z} \approx \left(h + 4\varepsilon\sigma T_A^{\,3}\right)D \quad , \qquad for \;\; z = 0 \, , \text{ and} \tag{10b}$$

$$k\frac{\partial D}{\partial z} \approx \varepsilon\sigma\left(T_C^{\,4} - T_A^{\,4}\right) - 4\varepsilon\sigma T_A^{\,3}D \quad , \quad for \;\; z = L \, , \tag{10c}$$

where T_A is the ambient temperature of the room and window mounting flange, T_C is the effective temperature inside the chamber, D is the diameter of the window opening in the chamber, L is the window thickness, k is the thermal conductivity, ε the emissivity, h the air-glass film coefficient for convective transfer, and σ the Stephan-Boltzman constant. Particular solutions of the diffusion equation have the form

$$D = \left[F\cos(Bz) + G\sin(Bz)\right]J_0(Ar)e^{-\alpha^2\left(A^2+B^2\right)t} \quad . \tag{11}$$

A steady-state solution occurs if $A^2 + B^2 = 0$, in which case we have

$$D_0 = \sum_{n=1}^{\infty}\left[F_n\cosh\left(A_n z\right) + G_n\sinh\left(A_n z\right)\right]\cdot J_0\left(A_n r\right) \quad , \tag{12}$$

where the A_n have been chosen to satisfy the first boundary condition:

$$A_n = \frac{2a_n}{D} \quad , \qquad J_0\left(a_n\right) = 0 \quad , \; n = \; 1, \; 2, \; 3, \; \ldots \tag{13}$$

and the constants F_n and G_n are derived by matching the boundary conditions at $z = 0$ and $z = L$.

The foregoing steady-state temperature distribution exists within the window after the thermal shroud has been cold for many hours. The distribution (12) was evaluated with the best available estimates of all of the constants, and is shown in Figure 3. The effective temperature inside the chamber (T_C) was adjusted until the solution matched thermocouple measurements made at two points on the outside of the window. This was needed because the chamber actually contained a complicated assemblage of equipment with a variety of temperatures, emissivities, and view factors to the window. The resulting net radiated power approximately agreed with that estimated from the internal chamber geometry and temperatures.[4]

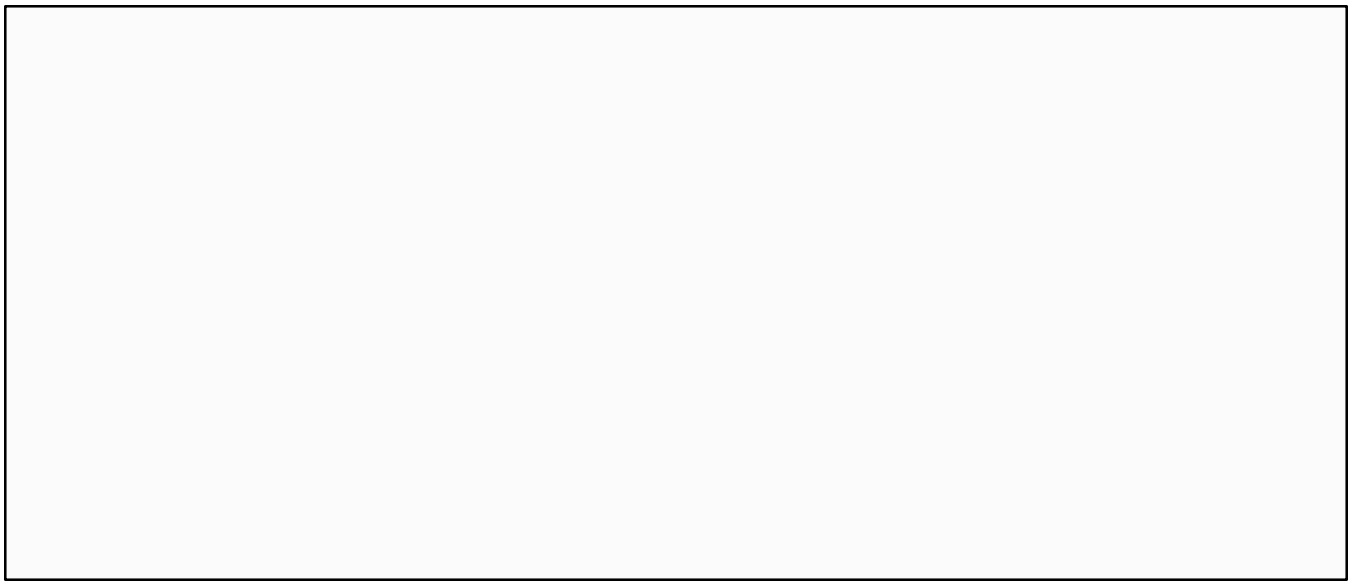

Figure 3. Steady-state temperature distribution within the vacuum chamber window. Values of constants for this case are T_A = 20.0° C, T_C = 271 K, and T_H = 20.0° C. The differential temperature (T - T_A) contours are labeled in °C.

The optical path difference across the window (equation (7)) has been evaluated for the temperature distribution shown in Figure 3, and the result is plotted in Figure 4.

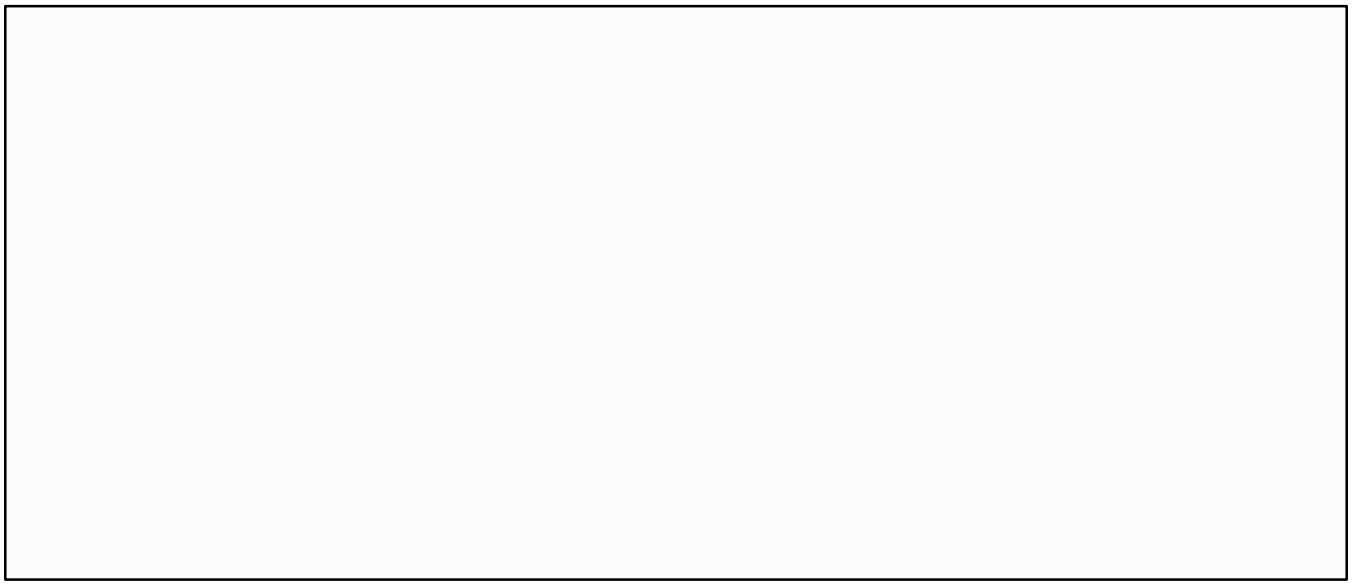

Figure 4. Optical path difference across the window resulting from the temperature distribution shown in Figure 3.

Since the optical power induced in the window by the radial temperature gradients had a significant effect on our calibration tests, we sought a means to reduce those gradients. It was expected that application of heat to the outside face of the window would balance the heat radiating into the chamber. The goal was to achieve a temperature distribution in the window that had a small radial gradient, though a larger axial gradient. This should greatly reduce the optical power of the window.

A heated plate placed in front of the window was expected to provide a uniform heat flux to produce the desired temperature gradients. The new configuration alters one of the boundary conditions (10b) for solving the diffusion equation. We now have

$$k\frac{\partial D}{\partial z} \approx \left(h + 4\varepsilon\sigma T_A^{\,3}\right)D - f_a\varepsilon\sigma\left(T_H^{\,4} - T_A^{\,4}\right) \qquad @ \;\; z = 0 \;\; , \tag{14}$$

where

T_H = the temperature of the heated plate, and
f_a = a view factor between the window and the plate 0.8.

The steady-state temperature solution has the same form as before (equation (12)), but the values of the constants F_n and G_n are modified. In general, we find

$$F_n = \frac{A_n K_1 + D_n K_2}{\left[A_n C_n + \left(\frac{h}{k} + K_0\right)D_n\right]} \cdot \frac{2}{a_n J_1(a_n)} \;\; , \tag{15}$$

$$G_n = \frac{\left(\frac{h}{k} + K_0\right)K_1 - C_n K_2}{\left[A_n C_n + \left(\frac{h}{k} + K_0\right)D_n\right]} \cdot \frac{2}{a_n J_1(a_n)} \;\; , \tag{16}$$

where we define the constants

$$K_0 = \frac{4\varepsilon\sigma T_A^{\,3}}{k} \;\; , \tag{17}$$

$$K_1 = \frac{\varepsilon\sigma}{k}\left(T_C^{\,4} - T_A^{\,4}\right) \, , \tag{18}$$

$$K_2 = \frac{\varepsilon\sigma}{k}\, f_a\left(T_H^{\,4} - T_A^{\,4}\right) \, , \tag{19}$$

$$C_n \equiv A_n \sinh(A_n L) + K_0 \cosh(A_n L) \;\; , \tag{20}$$

and

$$D_n \equiv A_n \cosh(A_n L) + K_0 \sinh(A_n L) \;\; . \tag{21}$$

The steady-state temperature distribution in the window, and the optical path difference across the window are plotted in Figure 5, for the condition in which the window receives as much heat flux from the external heater plate as it radiates into the chamber. This steady-state solution is a linear superposition of the original solution (12) and a similar solution having the z coordinate reversed and the sign of the temperature changed:

$$D_H(r,z) = D_0(r,z) - D_0(r,-z) \;\; . \tag{22}$$

a)

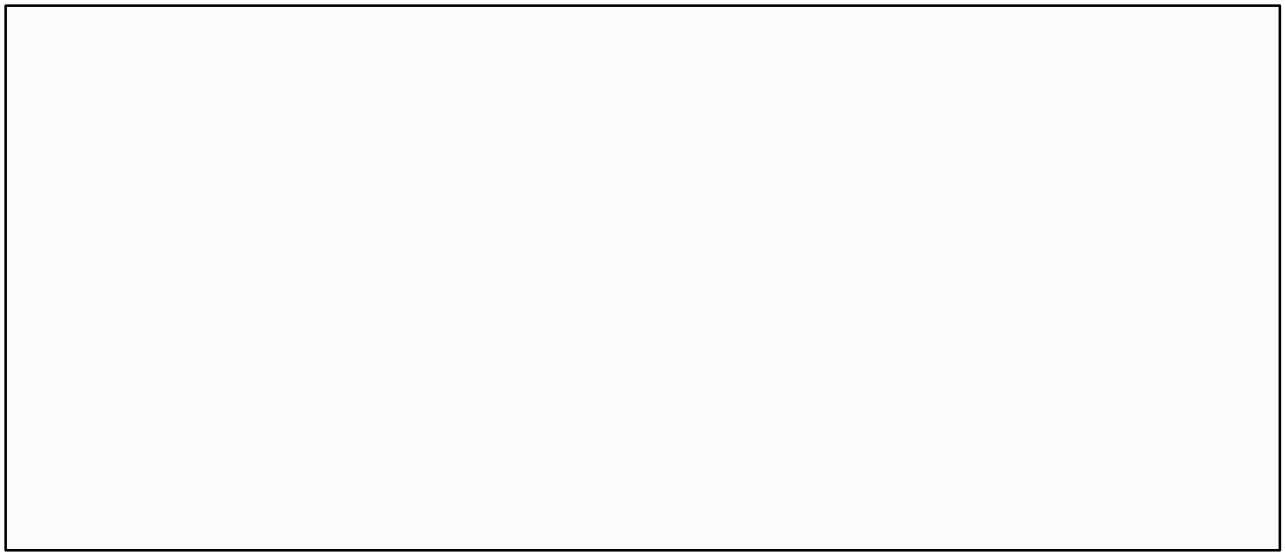

b)

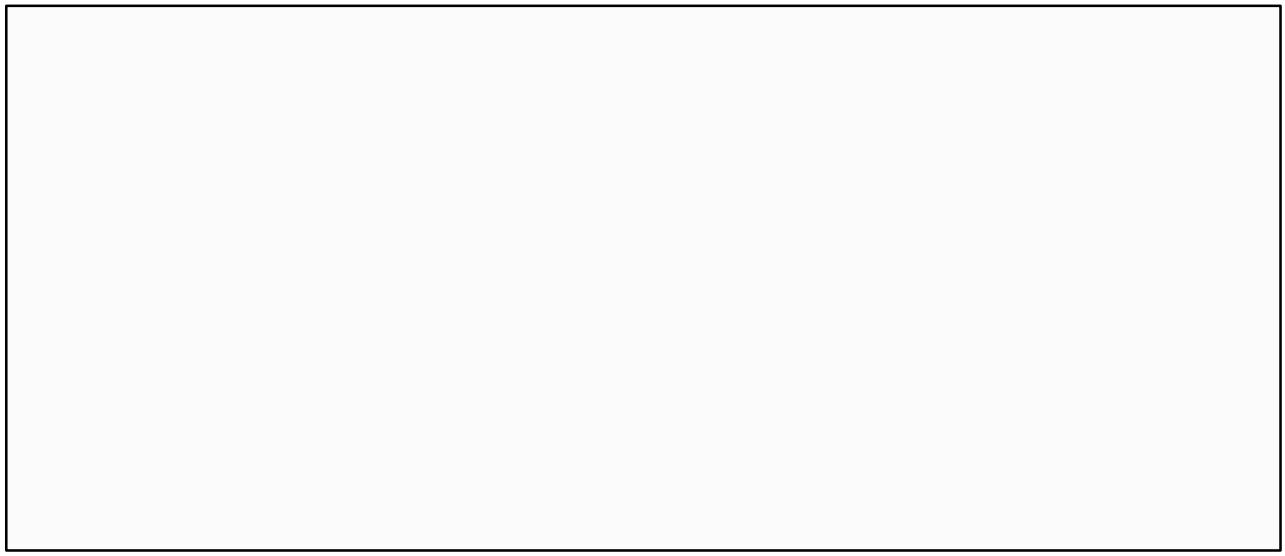

Figure 5. Results of placing a black plate in front of the window, heated to 42.5° C. a) Steady-state temperature distribution within the vacuum chamber window. b) Optical path difference across the window. Only the center region, to a radius of 6.25 cm, is seen by the ALI.

In order to estimate how the optical power of the window will change when the heater is removed, we desire the complete, time-dependent solution of the diffusion equation (5). The general solution for this geometry may be written as

$$D(r,z,t) = D_{0H}(r,z) + D_1(r,z,t) \quad , \tag{23}$$

where D_{0H} is the steady-state solution. Since the final state is the same as in the unheated case, $D_{0H} = D_0$. The transient part of the solution is

$$D_1(r,z,t) = \sum_{n=1}^{\infty} J_0(A_n r) e^{-a^2 A_n^2 t} \left[\tfrac{1}{2} H_{n0} + \sum_{j=1}^{\infty} H_{nj} \cos\left(pj \frac{z}{L} \right) e^{-a^2 \left(\frac{pj}{L} \right)^2 t} \right] \tag{24}$$

The coefficients H_{nj} are to be evaluated by matching the initial condition, which is the heated steady-state solution (22):

$$D(r,z,t=0)=D_0(r,z)-D_0(r,-z) \quad , \tag{25}$$

where D_0 is the unheated steady-state solution. After the heater is removed, the distribution approaches D_0. Thus the initial condition to be matched is

$$D_1(r,z,t=0)=-D_0(r,-z) \quad , \tag{26}$$

From equations (12), (24), and (26), we obtain

$$H_{nj}=-\frac{2A_nL}{(A_nL)^2+(pj)^2}\left\{F_n(-1)^j\sinh(A_nL)+G_n\left[(-1)^j\cosh(A_nL)-1\right]\right\} \quad . \tag{27}$$

The longest time constant in the transient solution is that for $n = 1$, $j = 0$:

$$t_{10}=\frac{1}{a^2A_1^2}=\frac{1}{a^2}\left(\frac{D}{2a_1}\right)^2=\frac{D^2}{9.6192a^2} \quad , \tag{28}$$

which in the present case has the value 79.7 minutes. The next longest time constant is 15.1 minutes, and only nine of the constants are greater than two minutes.

4.3. Reduction of window optical power

In order to measure the optical power of the window, the Zygo Mark IV interferometer was set up to measure the relative optical paths through the window. The setup is depicted in Figure 6. Figure 7 shows the Zygo monitor displays. The Zygo beam was directed normal to the window by a large, flat mirror that was temporarily mounted in front of the window for that purpose. Fringes were formed between the beams reflected from the front and back surfaces of the window. The Zygo was used to compute directly the optical power and residual wavefront error of the window (in HeNe waves across its 6-inch aperture). Typical power readings with the chamber interior cold were –0.75 waves p-v, with a residual WFE of 0.01 waves rms. Initially, a heat gun was applied to the window, and the fringes were seen to change, confirming that the thermo-optic effect was being observed.

Next, a blackened aluminum plate was arranged to fit in front of the window, which had foil heaters applied to its insulated back side. Thermocouples were also applied to its front side, facing the window. Application of current to the heaters raised the plate to a controlled temperature, and warmed the front of the window by radiation and convection.

Figure 6. Arrangement of Zygo interferometer for measurement of the window optical power. The turning flat mirror is just in front of the vacuum window. The monitor at the left displays the window fringes, while the one on top of the Zygo chassis shows the analyzed optical figure. Also seen, hanging below the window, is the insulated heating plate.

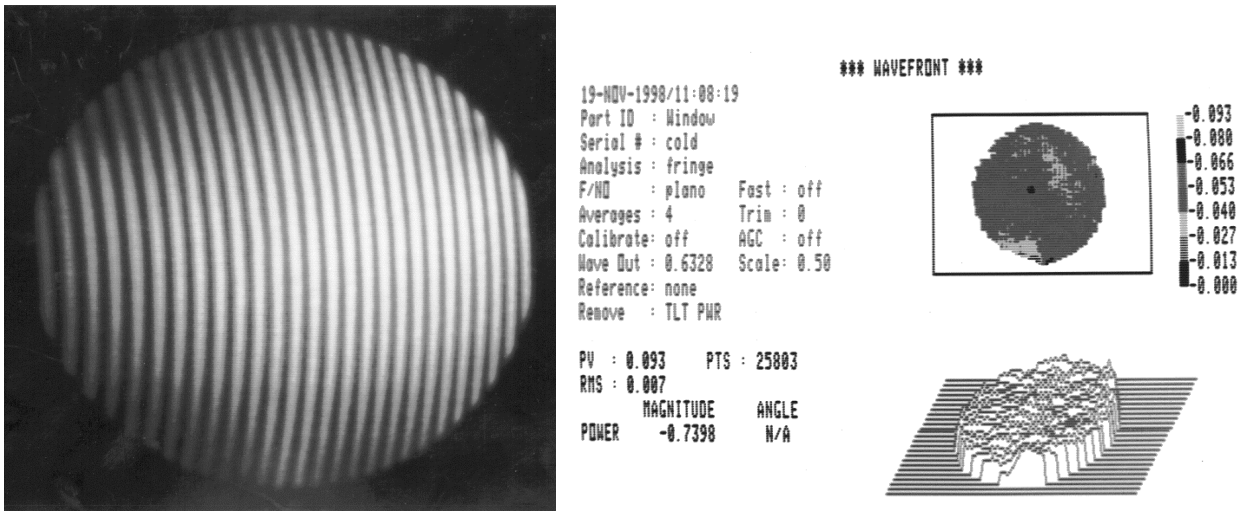

Figure 7. Zygo monitor displays: the fringes are shown on the left, and the residual wavefront, with power removed, is shown on the right.

While the OPD of the window could be reduced to ~ 0.015 HeNe waves ($1/f \sim -8 \times 10^{-7}$ diopters) with this technique, it is necessary to remove the heater plate in order to perform any optical measurements. As soon as we do so, the optical figure

begins to change toward the unheated condition shown in Figure 3. A series of Zygo measurements were made after heating the window for several hours, then removing the plate. The optical power of the window as a function of time since heater removal is plotted in Figure 8.

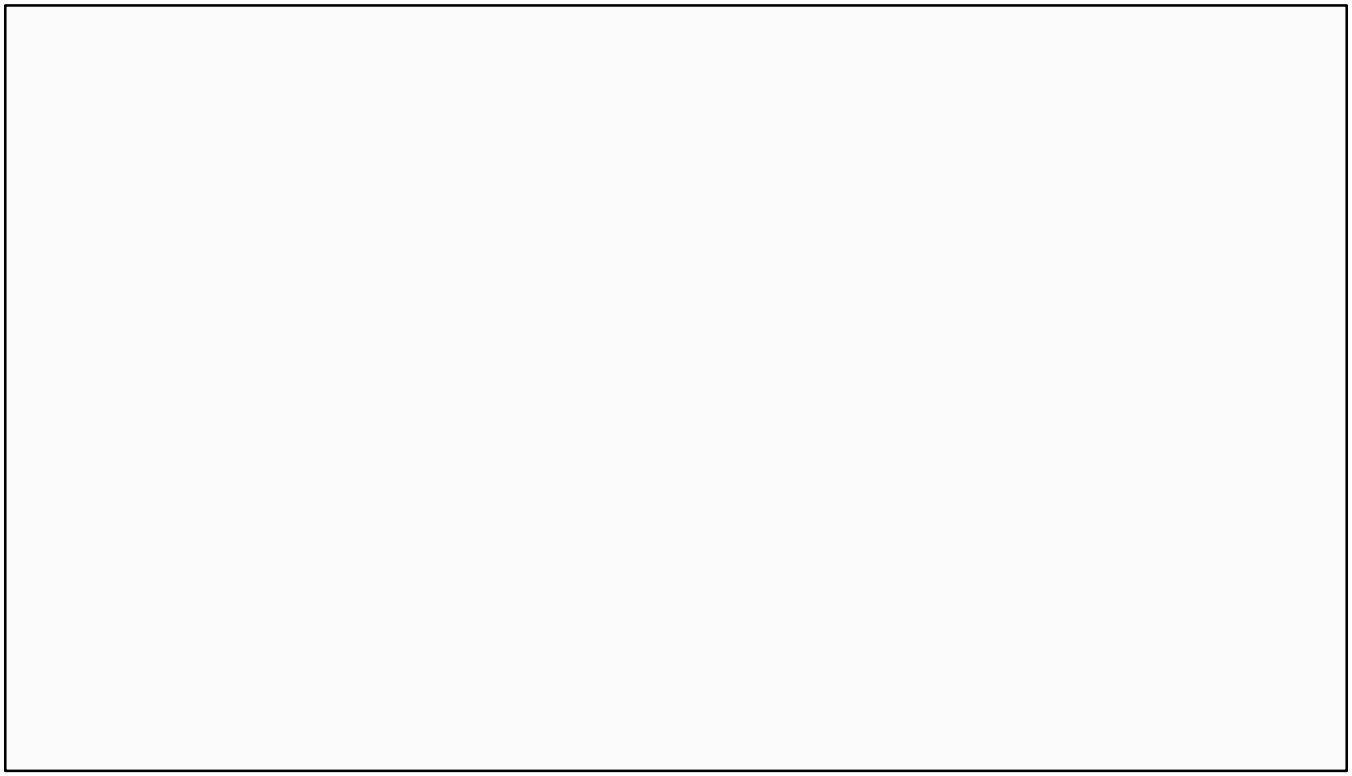

Figure 8. Optical power of the window *vs*. time since removal of the heater plate. The several series of data points represent Zygo measurements. The curves are derived from the time-dependent solution of the diffusion equation, with some parameters adjusted to match the measurements.

The temporal behavior seen in figure 8 shows that only a short interval is available after removal of the heater, before the window develops an excessive optical power. The initial rise toward positive power, followed by a slow fall, was first observed in the measurements and later confirmed with the time-dependent thermal diffusion solution.

4.4. Compensation for window optical power

The preceding section has shown that the thermally-induced optical power of the window can be removed by special thermal controls. For the spatial calibrations of the ALI however, it was not practical to use this technique. Instead, the Zygo interferometer was used to measure the power of the window before a series of tests, and a compensating power was added to the collimator by moving the test targets axially a short distance from the focal point. The focus adjustment is given by

$$Dz = \frac{f_c^{\,2}}{l - f_c - f_w} \approx -\frac{f_c^{\,2}}{f_w} \quad , \tag{29}$$

where

f_c = the focal length of the collimator,
f_w = the focal length of the window, and
l = the distance from the collimator primary mirror to the window.

As a check, the window power was measured after the series of tests, and found to be essentially unchanged.

5. SUMMARY

To calibrate the Advanced Land Imager (ALI) instrument of the EO-1 satellite under normal operating conditions, the instrument was placed in a thermal vacuum chamber. The window of the chamber had little effect on the optical quality of the calibrating beam until the thermal shroud within the chamber was cooled. Then, it developed a significant amount of optical power, primarily as a result of the thermo-optic coefficient (dn/dT) of the fused silica. A critical part of the spatial calibrations was to establish that the instrument would remain in correct focus at all times. Hence, the power of the window had to be measured, and either removed or compensated.

We have analyzed the temperature distribution in the window for a variety of conditions, by solving the diffusion equation. The optical power derived from those solutions agreed with that measured with a Zygo interferometer. It was demonstrated that the power could be reduced to an insignificant level by applying heat to the window in the right way. If time and space would permit, a radiant heater inside the chamber might remove all thermal gradients. In the case of the ALI spatial calibrations, the window was left to assume a small but steady optical power, and a compensating offset was applied to the test targets at the focus of the collimator.

6. ACKNOWLEDGEMENTS

The author wishes to thank the many staff members of MIT Lincoln Laboratory who assisted in this work. In particular, I thank Dr. Dave Nathanson and Dr. Donald E. Lencioni for helpful discussions of the present subject. Bert Willard set up the collimator and performed the Zygo measurements. Dr. Jeff Mendenhall measured the spectral transmission and took a major part in the calibration tests.

7. REFERENCES

1. Vukobratovich, D., "Optomechanical Design Principles," Ch. 2 in *Handbook of Optomechanical Engineering,* Ahmad, A., Ed., CRC Press, 1997.

2. Vukobratovich, D., "Optomechanical System Design," Ch. 3 in *The Infrared and Electro-Optical Systems Handbook, Vol. 4,* ERIM, Ann Arbor, 1993.

3. Klein, C. A., et al., "ZnS, ZnSe, and ZnS/ZnSe windows: their impact on FLIR system performance," *Optical Engineering*, Vol 25, pp. 519-531, 1986.

4 . D. Nathanson, private communication.